PROCEEDINGS OF SCIENCE

Neutron source-based event reconstruction in the JUNO detector

Akira Takenaka[a,*] **on behalf of the JUNO collaboration**

[a] *Tsung-Dao Lee Institute, Shanghai Jiao Tong University, No.520 Shengrong Road, Shanghai, China*

E-mail: akira.takenaka@sjtu.edu.cn

The Jiangmen Underground Neutrino Observatory (JUNO) is the largest underground liquid scintillator experiment in the world, currently under construction in southern China. JUNO aims to determine the neutrino mass ordering as its primary experimental goal by measuring the energy spectrum of reactor neutrinos. Its central detector consists of 20-kton liquid scintillator and more than 17,000 20-inch photomultiplier tubes. Vertex reconstruction and particle identification capability are important components in the event selection to suppress the backgrounds of the reactor neutrino events. The former is also crucial to understand the non-uniform energy response of the detector to achieve $3\%/\sqrt{E\ [\mathrm{MeV}]}$ of the energy resolution. In this proceedings paper, a data-driven method of reconstructing the event vertex position as well as separating positron and α/fast-neutron is discussed. Both of the algorithms can be developed with the radioactive neutron (Americium-Carbon) source which is planned to be regularly deployed to calibrate the JUNO detector responses. We will present the detailed methodology and reconstruction performances using the JUNO detector simulation.

38th International Cosmic Ray Conference (ICRC2023)
26 July - 3 August, 2023
Nagoya, Japan

ICRC2023
38th International Cosmic Ray Conference
The Astroparticle Physics Conference

*Speaker

PoS(ICRC2023)1146

1. Introduction

Neutrino oscillation [1, 2] is a phenomenon in which one neutrino flavor among the three flavors (ν_e, ν_μ, ν_τ) spontaneously changes to another during its propagation. A number of experiments [3–8] have confirmed that there are three neutrino mass eigenstates through observing this phenomenon. However, the large/small relation among the three mass eigenvalues, $m_{1\sim3}$, is not yet fully determined, leaving the two possibilities, normal ordering ($m_1 < m_2 < m_3$) or inverted ordering ($m_3 < m_1 < m_2$). Some prospective theories indicate that this neutrino property could be a key to reveal the origin of the baryon asymmetry (matter dominant) of the universe, such as leptogenesis [9], baryogenesis via neutrino oscillation [10].

The JUNO detector in Jiangmen, China [11], is the world's largest underground liquid scintillator (LS) detector shown in Figure 1, expected to start data taking in 2024. The 20 kton LS volume in a spherical acrylic vessel with a radius of 17.7 m works as a neutrino target, viewed by about 17,600 20-inch photomultiplier tubes (PMTs) and 25,600 3-inch PMTs to detect scintillation light from charged particles inside the LS volume to measure their deposited energy. The acrylic vessel and PMTs are strengthened by the stainless steel structure and immersed in the water region. JUNO will detect electron antineutrinos ($\bar{\nu}_e$) from nuclear power plants (NPPs), located about 53 km away from the detector, through the inverse beta decay ($\bar{\nu}_e + p \rightarrow e^+ + n$) in the LS volume. Some of the $\bar{\nu}_e$'s generated at NPPs oscillate (change) into other flavor neutrinos during their flight, and the oscillation probability depends on the neutrino energy as well as the true neutrino mass ordering. Consequently, the sign of the mass ordering appears in the positron deposited energy spectrum produced by surviving $\bar{\nu}_e$'s.

This proceeding mainly discusses the vertex reconstruction and particle identification algorithms, and the precise vertex reconstruction is one of the key points to correct the non-uniformity of the energy scale inside the detector and also to define the fiducial volume to reduce the influence by radioactive (external) backgrounds. Eliminating the α particles and fast neutrons based on the particle identification algorithm can also help to reduce the amount of the backgrounds in the reactor neutrino analysis. We have developed the vertex and particle identification algorithms using the JUNO offline simulation software [12] and present the results with the Monte-Carlo simulation.

2. Calibration Systems in JUNO

A variety of calibration source deployment systems [13] will be installed in the JUNO detector as depicted in Figure 2, making it possible to calibrate the position-dependent detector response. Every system can place a radioactive γ-ray/neutron source (^{241}Am^{13}C source [14], 6.1 MeV γ-ray from ^{16}O* and 2.2 MeV γ-ray from neutron capture in LS) within its peculiar movable coverage.

The movable calibration sources also provide a chance to develop an event vertex reconstruction tool in a data-driven way because the source location can be regarded as "a true event location" in the calibration data, and the PMT response can be modeled as a function of the known event location. The vertex and particle identification algorithms have been developed using the ^{241}Am^{13}C neutron source calibration events along the central axis with the automatic calibration unit system. Besides the ^{241}Am^{13}C source events, uniformly distributed 2.2 MeV γ-ray events inside the detector are also exploited to further improve the vertex reconstruction algorithm. Such 2.2 MeV γ-ray events

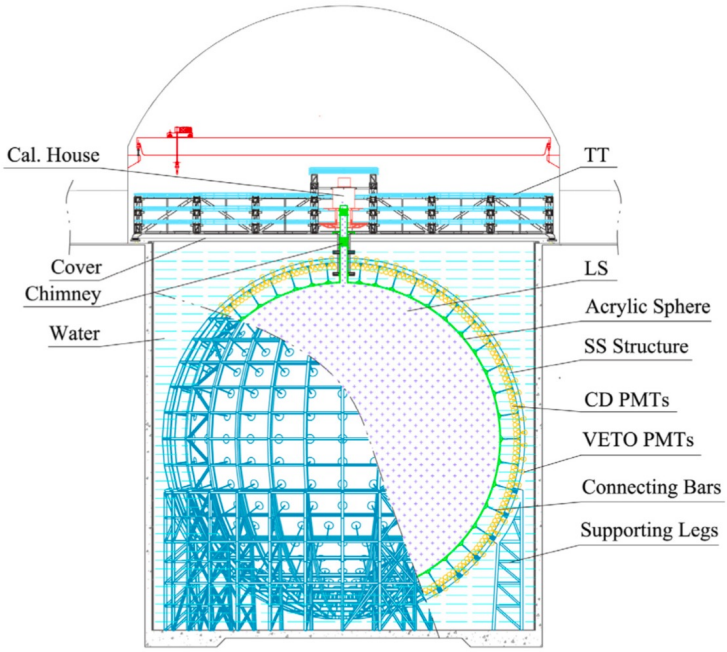

Figure 1: A schematic of the JUNO detector. Taken from [11].

are expected to be available from cosmogenic neutrons, which are produced as cosmic-ray muon spallation products and captured on hydrogen nuclei in LS.

3. Vertex Reconstruction and Particle Identification Algorithm

3.1 Vertex Reconstruction Algorithm

The vertex position of each event inside the LS volume is reconstructed by maximizing the following likelihood (L):

$$
\begin{aligned}
L &= \prod_{j}^{\text{Unhit PMTs}} P_j^q(\text{unhit}|\mu_j^{\text{exp}}) \prod_{i}^{\text{Hit PMTs}} P_i^q(Q_i^{\text{obs}}|\mu_i^{\text{exp}}) P_i^t(t_{i,\text{residual}}|R, \theta_{i,\text{PMT}}, Q_i^{\text{obs}}, \text{Total Charge}),\\
\mu_i^{\text{exp}} &= \mu_{i,0}^{\text{exp}}(R, \cos\Theta, \theta_{i,\text{PMT}}) \times \text{Total Charge},\\
t_{i,\text{residual}} &= t_i^{\text{first hit time}} - \text{T.O.F.}(x, y, z) - t_0,\\
R &= \sqrt{x^2 + y^2 + z^2},\\
\text{Total Charge} &= \sum_{i}^{\text{Hit PMTs}} Q_i^{\text{obs}}
\end{aligned}
$$

where $t_i^{\text{first hit time}}$ is the first photon hit time at the ith PMT in the event timing window, (x, y, z) denotes the event position, t_0 is the event time, Θ specifies the event location in terms of the zenith angle , $\theta_{i,\text{PMT}}$ is the relative angle between the vertex position and the ith PMT location (see Figure 3), T.O.F. is the time-of-flight of the photon between the event vertex position and PMT

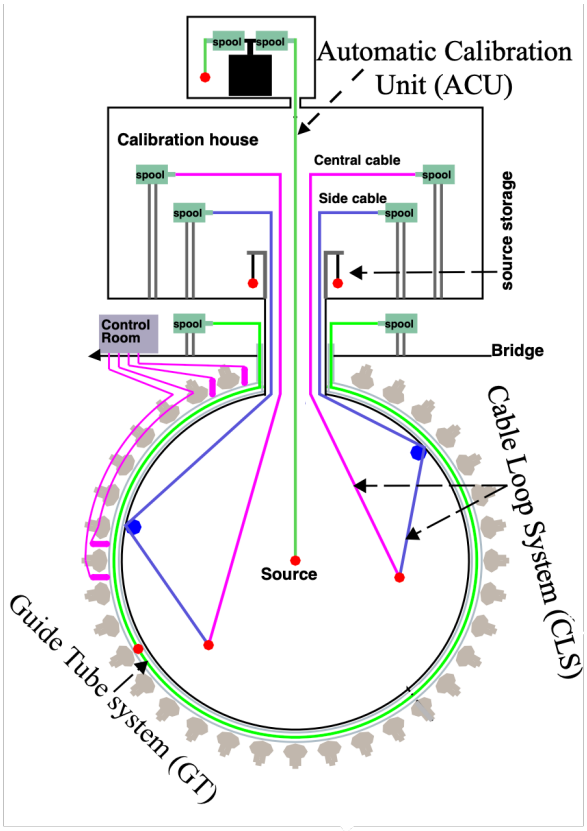

Figure 2: A schematic of the JUNO calibration system. Automatic calibration unit (ACU) can place the calibration source along the detector central axis. With cable loop system (CLS), a calibration source can be deployed at positions apart from the detector central axis in one specific vertical plane. Guide tube is a tube attached to the outer surface of the acrylic sphere, and a source can be deployed along the tube. Taken from [13].

location, Q_i^{obs} is the observed charge at the ith PMT, μ_i^{exp} is the expected charge at ith PMT, and P^q (P^t) is the charge (timing) probability density function (P.D.F.).

3.2 Timing P.D.F.

The timing profile of the scintillation light emission is calibrated and tabulated using the ^{241}Am^{13}C source events along the central axis of the detector. The calibration source location is used for the time-of-flight calculation, and position as well as observed charge dependence is taken into account in the timing P.D.F. building as a function of (R, $\theta_{i,\text{PMT}}$, Q_i^{obs}, Total Charge). An exemplary residual time distribution is shown in Figure 4.

3.3 Charge Map

Because the observed charge at individual PMT depends on the spacial relation ship between the vertex and PMT positions, charge prediction map has been prepared using the neutron samples uniformly distributed inside the detector. By subdividing the detector into many small volumes (voxels), the change of the observed charge value is captured and the charge map is also tabulated

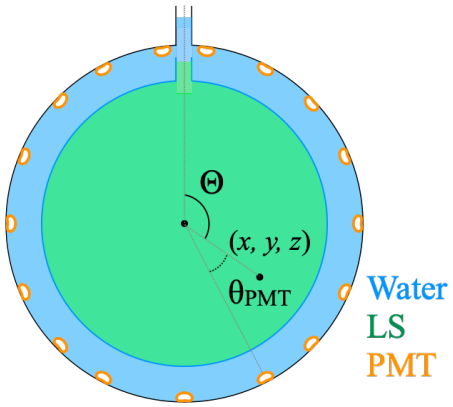

Figure 3: Coordinates used in the vertex and particle identification algorithm. The position is described as (x, y, z), Θ denotes the zenith angle of the vertex position and $\theta_{i,\mathrm{PMT}}$ is the relative angle between the vertex position and the PMT location.

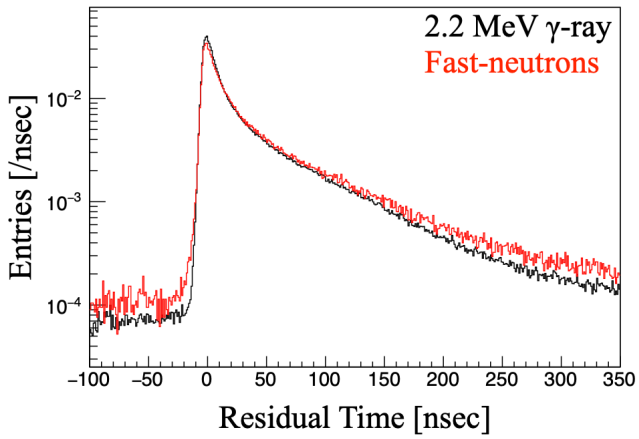

Figure 4: Exemplary plot for the timing P.D.F. used in the vertex reconstruction and particle identification algorithm.

as a function of $(R, \cos\Theta, \theta_{i,\mathrm{PMT}})$. When the charge map is build, each charge value is normalized by the total charge in each event to make the charge map energy independent. The event location of each neutron (2.2 MeV γ-ray) event is reconstructed by applying an independent time-based algorithm.

3.4 Charge P.D.F.

Charge probability density function is the probability of observing Q^{obs} with the given expected charge of μ^{exp}. In the photon counting measurement, the observed number of photons basically follows the Poisson distribution with the mean luminosity of μ. However, due to the charge amplification performance of the 20-inch PMT [15], this relationship does not work well in the event reconstruction stage. Therefore, this study constructs the charge P.D.F. (distribution) as a function of mean charge value based on the laser samples. By changing the laser intensity, charge

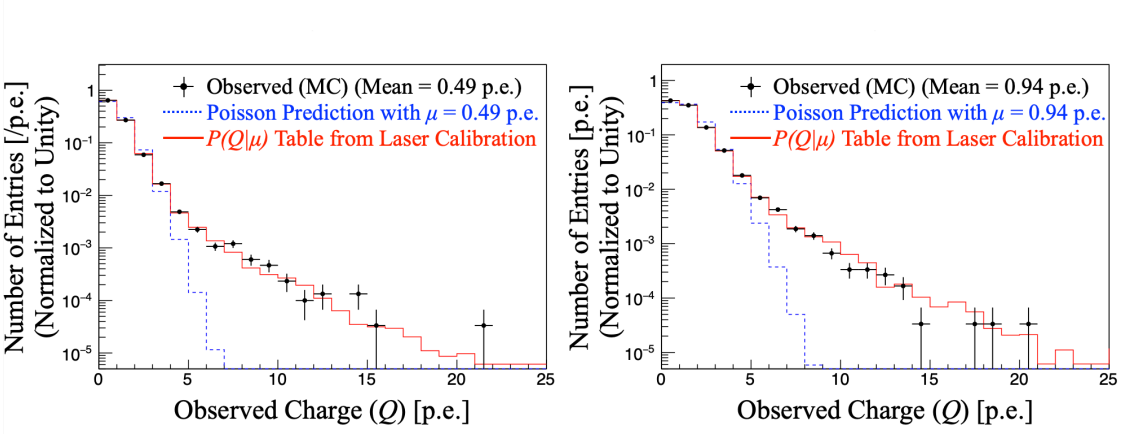

Figure 5: Exemplary plots for the observed charge distribution, Poisson distribution and the predictions from the charge P.D.F.

distributions at different mean charge values can be directly calibrated. A few exemplary plots of the observed charge distribution, Poisson distribution and the predictions from the charge P.D.F. are shown in Figure 5.

3.5 Particle Identification Algorithm

The scintillation light profile depends on the particle type as shown in Figure 4. Almost pure fast-neutron samples are available from the ^{241}Am^{13}C source events, and the timing P.D.F. for fast neutrons are build separately. After the event vertex position is determined the likelihood for the γ-ray assumption and α/fast-neutron individually. By taking the difference of $-\log L$ between the two assumptions, the particle identification is done.

4. Results

The vertex resolutions for positron events have been evaluated at different energies and are shown in Figure 6. The radial vertex resolution around 1 MeV energy deposition point is estimated to be better than 9 cm.

As for the particle identification algorithm, it is found that about 68% (36%) of α particles (fast-neutrons) can be rejected while keeping the signal efficiency as high as about 99%. The separation between the position events and α particles events are also shown in Figure 6.

5. Conclusion

We have developed the vertex reconstruction and particle identification algorithms based on radioactive neutron source as well as cosmogenic neutron events. A variety of the parameter inputs such as timing P.D.F., charge map, and charge P.D.F., are derived from the calibration events. Based on the detector simulation study, the vertex resolution of the lowest energy positron events has been estimated to be about 9 cm and the algorithm is capable to reject about 68% (36%) of the α particle (fast-neutron) events with keeping the 99% of the signal positron events.

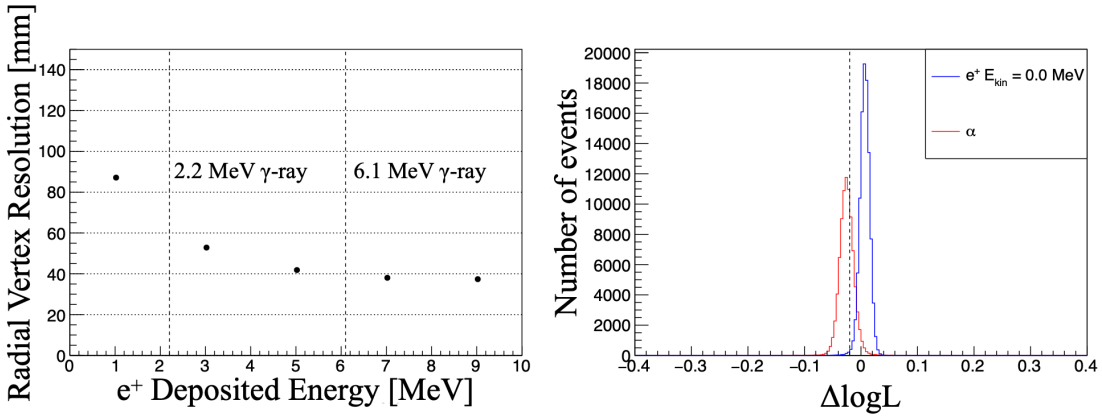

Figure 6: Left: Radial vertex resolutions for position events as a function of the positron deposited energy. Right: $\Delta \log L$ distribution for the particle identification for positron events with the kinetic energy of 0 MeV and α particle events with the kinetic energy from 1 to 10 MeV. The vertical dashed line denotes the separation threshold.

References

[1] Z. Maki, M. Nakagawa and S. Sakata, Prog. Theor. Phys. 28, 870 (1962).

[2] B. Pontecorvo, Sov. Phys. JETP 26, 984 (1968).

[3] Y. Fukuda *et al.* (Super-Kamiokande), Phys. Rev. Lett. 81, 1562 (1998).

[4] Q. R. Ahmad *et al.* (SNO), Phys. Rev. Lett. 89, 011301 (2002).

[5] K. Eguchi *et al.* (KamLAND), Phys. Rev. Lett. 90, 021802 (2003).

[6] Y. Abe *et al.* (Double Chooz), Phys. Rev. Lett. 108, 131801 (2012).

[7] F. P. An *et al.* (Daya Bay), Phys. Rev. Lett. 108, 171803 (2012).

[8] J. K. Ahn *et al.* (RENO), Phys. Rev. Lett. 108, 191802 (2012).

[9] M. Fukugita, and T. Yanagida, Phys. Lett. B 174, 45 (1986).

[10] E. Kh. Akhmedov, V. A. Rubakov, and A. Yu. Smirnov, Phys. Rev. Lett. 81, 1359 (1998).

[11] A. Abusleme *et al.* (JUNO), Prog. Part. Nucl. Phys. 123, 103927 (2022).

[12] T. Lin *et al.*, Eur. Phys. J. C 83, 382 (2023).

[13] A. Abusleme *et al.* (JUNO), J. High Energ. Phys. 2021, 4 (2021).

[14] J. Liu *et al.*, Nucl. Instrum. Meth. A 797, 260 (2015).

[15] H.Q. Zhang *et al.* JINST 16, T08009 (2021).